

# Soft Gluon Resummation in $t$ -channel single top quark production at the LHC

---

Qing-Hong Cao<sup>1,2,3</sup>, Peng Sun<sup>4</sup>, Bin Yan<sup>5</sup>, C.-P. Yuan<sup>5</sup>, Feng Yuan<sup>6</sup>

<sup>1</sup>*Department of Physics and State Key Laboratory of Nuclear Physics and Technology, Peking University, Beijing 100871, China*

<sup>2</sup>*Collaborative Innovation Center of Quantum Matter, Beijing 100871, China*

<sup>3</sup>*Center for High Energy Physics, Peking University, Beijing 100871, China*

<sup>4</sup>*Department of Physics and Institute of Theoretical Physics, Nanjing Normal University, Nanjing, Jiangsu, 210023, China*

<sup>5</sup>*Department of Physics and Astronomy, Michigan State University, East Lansing, MI 48824, USA*

<sup>6</sup>*Nuclear Science Division, Lawrence Berkeley National Laboratory, Berkeley, CA 94720, USA*

*E-mail:* [qinghongcao@pku.edu.cn](mailto:qinghongcao@pku.edu.cn), [pengsun@msu.edu](mailto:pengsun@msu.edu), [yanbin1@msu.edu](mailto:yanbin1@msu.edu),  
[yuan@pa.msu.edu](mailto:yuan@pa.msu.edu), [fyuan@lbl.gov](mailto:fyuan@lbl.gov)

**ABSTRACT:** We present a detailed phenomenological study of the multiple soft gluon radiation for the  $t$ -channel single top and anti-top quark production at the Large Hadron Collider (LHC). By applying the transverse momentum dependent factorization formalism, large logarithms introduced by small total transverse momentum  $q_{\perp}$  of the single-top (anti-top) plus one-jet final state system are resummed to all orders in the expansion of the strong interaction coupling at the accuracy of Next-to-Leading Logarithm. We discuss various kinematical distributions which are sensitive to this effect and find that soft gluon radiation become more important when the final state jet is required to be in the forward region. We show that the main difference from PYTHIA prediction lies on the inclusion of the exact color coherence effect between the initial and final states in our resummation calculation. We further propose to apply the experimental observable  $\phi^*$  to test the effect of multiple gluon radiation in the single-top and anti-top events. The bottom quark mass effect and jet rapidity distribution are also discussed.

**KEYWORDS:** QCD, Single Top-Quark Production, Resummation

---

## Contents

<b>1</b>	<b>Introduction</b>	<b>1</b>
<b>2</b>	<b>Factorization and Resummation</b>	<b>2</b>
<b>3</b>	<b>Phenomenology</b>	<b>8</b>
<b>4</b>	<b>Conclusions</b>	<b>17</b>

---

## 1 Introduction

Top quark has its mass around the electroweak symmetry breaking scale and is expected to play an important role of testing the Standard Model (SM) and provide a window to new physics (NP) of beyond the SM. At the CERN Large Hadron Collider (LHC), top quarks can be produced by the electroweak gauge interaction [1–4]. Its cross section is proportional to the  $Wtb$  coupling [5–18] and Cabibbo-Kobayashi-Maskawa (CKM) matrix element  $V_{tb}$  [9, 19]. Hence, it offers a promising way to constrain various  $Wtb$  anomalous couplings, induced by NP, or determine  $V_{tb}$  without assuming the generation of quarks. Furthermore, top quarks produced from the electroweak process are highly polarized, and the degree of polarization of the top quark in the single top quark process events can be used to discriminate New Physics models at the LHC [20–36], e.g. the  $W'$  gauge boson from  $G(221)$  models [29–31], new heavy fermions [34–36] and charged scalars [32, 33]. In addition, single top quark production can also be used to measure top quark mass [37, 38] and constrain the light quark PDFs [39]. Therefore, a precise study of both the inclusive and differential cross sections of single top quark events is vital to test the SM and search for NP.

At the LHC, single top quark is predominantly produced through  $t$ -channel mode. The total and differential cross sections have been measured by the ATLAS and CMS collaborations at  $\sqrt{s} = 7$  TeV [40, 41],  $\sqrt{s} = 8$  TeV [42, 43] and  $\sqrt{s} = 13$  TeV [44, 45]. These results are consistent with the SM predictions [46–48]. The single top quark production and decay in hadron collision at the next-to-leading order (NLO) accuracy in QCD correction, has been known for many years [49–66]. Recently, the dominant part of the next-to-next-to-leading order (NNLO) QCD correction to predicting the detailed kinematical distributions, including proper spin correlations, in  $t$ -channel single top events, has been discussed in Refs. [46–48]. Beyond the fixed order calculation, the threshold resummation technique is also widely discussed to improve the inclusive production rate of the single-top quark event in the literatures [67–72]. Furthermore, the accuracy of transverse momentum distribution of the top

quark could also be improved by summing over large logarithms  $\ln(m_t^2/s_4)$  with  $s_4 \rightarrow 0$ , where  $s_4 = \hat{s} + \hat{t} + \hat{u} - m_t^2$ , in which  $\hat{s}$ ,  $\hat{t}$  and  $\hat{u}$  are the usual Mandelstam variables [67–72].

In a recent publication [73], we studied kinematical distributions of  $t$ -channel single top events by applying the transverse momentum ( $q_\perp$ ) resummation formalism to sum over large logarithms  $\ln(Q^2/q_\perp^2)$ , with  $Q \gg q_\perp$ , to all orders in the expansion of the strong interaction coupling ( $g_s$ ) at the next-to-leading-logarithm (NLL) accuracy. Here,  $Q$  and  $q_\perp$  are the invariant mass  $Q$  and total transverse momentum  $q_\perp$  of the single-top plus one-jet final state system, respectively. The  $q_\perp$  resummation technique is based on the transverse momentum dependent (TMD) factorization formalism [74], which has been widely discussed in the color singlet processes, such as Drell-Yan production [75, 76]. Extending the  $q_\perp$  resummation formalism to processes with more complex color structure are also discussed widely recently, e.g. heavy quark production [77–79], and processes involving multijets in the final state [73, 80–90]. For those processes, additional large logarithms, induced by soft gluon radiation from color coherence effects, need to be resummed via the modified  $q_\perp$  resummation formalism.

As shown on the Ref [73], the  $q_\perp$  spectrum of  $t$ -channel single top quark production strongly depends on the color coherence effects between the initial state and final state jets and the treatment of bottom quark mass in the resummation calculation. The sub-leading logarithms from soft gluon interaction play an even more important role when the final state jet is required to be in the forward region, which is identified as the  $t$ -channel single top signal region, where our resummation prediction is different with PYTHIA parton shower result. In the present paper, we present details of our results in Ref. [73]. In Sec. 2, we present the detail of our resummation calculation. Its phenomenology is discussed in Sec. 3. Our conclusion is given in Sec. 4.

## 2 Factorization and Resummation

We consider the process  $pp \rightarrow t(\bar{t}) + jet + X$  at the LHC. Using the TMD resummation formalism presented in Ref. [82], the differential cross section of the  $t$ -channel single top quark production process can be written as

$$\frac{d^4\sigma}{dy_t dy_J dP_{J\perp}^2 d^2q_\perp} = \sum_{ab} \left[ \int \frac{d^2\vec{b}}{(2\pi)^2} e^{-i\vec{q}_\perp \cdot \vec{b}} W_{ab \rightarrow tJ}(x_1, x_2, \mathbf{b}) + Y_{ab \rightarrow tJ} \right], \quad (2.1)$$

where  $y_t$  and  $y_J$  are the rapidities of the top quark and the final state jet, respectively;  $P_{J\perp}$  and  $q_\perp$  are the transverse momenta of the jet and the total transverse momentum of the top quark and the jet system, i.e.  $\vec{q}_\perp = \vec{P}_{t\perp} + \vec{P}_{J\perp}$ . The  $W_{ab \rightarrow tJ}$  term contains all order resummation contribution, in powers of  $\ln(Q^2/q_\perp^2)$ , and the inclusion of the  $Y_{ab \rightarrow tJ}$  term is to account for the part of fixed-order corrections which are not included in the expansion of the  $W_{ab \rightarrow tJ}$  term to the same order in strong coupling constant  $g_s$ . The variables  $x_1, x_2$  are momentum fractions of the incoming hadrons carried by the partons, with

$$x_{1,2} = \frac{\sqrt{m_t^2 + P_{t\perp}^2} e^{\pm y_t} + \sqrt{P_{J\perp}^2} e^{\pm y_J}}{\sqrt{S}}, \quad (2.2)$$

where  $m_t$  and  $S$  are the top quark mass and squared collider energy, respectively.

The above  $W$  term can be further written as

$$W_{ab \rightarrow tJ}(x_1, x_2, \mathbf{b}) = x_1 f_a(x_1, \mu_F = b_0/b_*) x_2 f_b(x_2, \mu_F = b_0/b_*) e^{-S_{\text{Sud}}(Q^2, \mu_{\text{Res}}, b_*)} e^{-\mathcal{F}_{NP}(Q^2, \mathbf{b})} \\ \times \text{Tr} \left[ \mathbf{H}_{ab \rightarrow tJ}(\mu_{\text{Res}}) \exp\left[-\int_{b_0/b_*}^{\mu_{\text{Res}}} \frac{d\mu}{\mu} \gamma^{s\dagger}\right] \mathbf{S}_{ab \rightarrow tJ}(b_0/b_*) \exp\left[-\int_{b_0/b_*}^{\mu_{\text{Res}}} \frac{d\mu}{\mu} \gamma^s\right] \right], \quad (2.3)$$

where  $Q^2 = \hat{s} = x_1 x_2 S$ , the hard scale of this process,  $b_0 = 2e^{-\gamma_E}$  with  $\gamma_E$  being the Euler constant 0.5772,  $f_{a,b}(x, \mu_F)$  are parton distribution functions (PDF) for the incoming partons  $a$  and  $b$ , and  $\mu_{\text{Res}}$  represents the resummation scale of this process. Here,  $b_* = \mathbf{b}/\sqrt{1 + \mathbf{b}^2/b_{\text{max}}^2}$  with  $b_{\text{max}} = 1.5 \text{ GeV}^{-1}$ , which is introduced to factor out the non-perturbative contribution  $e^{-\mathcal{F}_{NP}(Q^2, b)}$ , arising from the large  $\mathbf{b}$  region (with  $\mathbf{b} \gg b_*$ ) [91–94],

$$\mathcal{F}_{NP}(Q^2, \mathbf{b}) = g_1 \mathbf{b}^2 + g_2 \ln \frac{Q}{Q_0} \ln \frac{\mathbf{b}}{b_*}, \quad (2.4)$$

where  $g_1 = 0.21$ ,  $g_2 = 0.84$  and  $Q_0^2 = 2.4 \text{ GeV}^2$  [94]. In this study, we shall use CT14NNLO PDFs [95] for our numerical calculation. Hence, our resummation calculation should be consistently done in the General-Mass-Variable-Flavor (GMVR) scheme that the PDFs are determined. The bottom quark PDF is set to zero when the factorization scale  $\mu_F$  is below the bottom quark mass threshold, i.e.  $\mu_F < m_b$ . To properly describe the small  $q_\perp$  region (for  $q_\perp < m_b$ ), the S-ACOT scheme [96–99] is adopted to account for the effect from the (non-zero) mass of the incoming bottom quark in the hard scattering process. In Refs. [100–102], a detailed discussion has been given on how to implement the S-ACOT scheme in the  $q_\perp$  resummation formalism, for processes initiated by bottom quark fusion. In short, the S-ACOT scheme retains massless quark in the calculation of the hard scattering amplitude (of  $qb \rightarrow q't$ ), but with the (bottom quark) mass dependent Wilson coefficient  $C_{b/g}^{(1)}(x, \mathbf{b}, \mu_F)$ , to account for the contribution from gluon splitting into a  $b\bar{b}$  pair [100–102],

$$C_{b/g}^{(1)}(z, \mathbf{b}, m_b, \mu_F) = \frac{1}{2} z(1-z) \mathbf{b} m_b K_1(\mathbf{b} m_b) + P_{q/g}^{(1)}(z) \left[ K_0(\mathbf{b} m_b) - \theta(\mu_F - m_b) \ln \frac{\mu_F}{m_b} \right] \quad (2.5)$$

where the factorization scale  $\mu_F = b_0/\mathbf{b}$ ,  $K_0(z)$  and  $K_1(z)$  are the modified Bessel functions,  $P_{q/g}^{(1)}(z)$  is the gluon splitting kernel. This expression reduces to the massless result when  $1/\mathbf{b} \ll m_b$  [101],

$$C_{b/g}^{(1)}(z, \mathbf{b}, m_b = 0, \mu_F) = \frac{1}{2} z(1-z) - \ln \frac{\mu_F \mathbf{b}}{b_0} P_{q/g}^{(1)}(z). \quad (2.6)$$

The hard and soft factors  $\mathbf{H}$  and  $\mathbf{S}$  are expressed as matrices in the color space of  $ab \rightarrow tJ$ , and  $\gamma^s$  is the associated anomalous dimension of the soft factor. The Sudakov form factor

$\mathcal{S}_{\text{Sud}}$  resums the leading double logarithm and the sub-leading logarithms,

$$S_{\text{Sud}}(Q^2, \mu_{\text{Res}}, b_*) = \int_{b_0^2/b_*^2}^{\mu_{\text{Res}}^2} \frac{d\mu^2}{\mu^2} \left[ \ln \left( \frac{Q^2}{\mu^2} \right) A + B + D_1 \ln \frac{Q^2 - m_t^2}{P_{J\perp}^2 R^2} + D_2 \ln \frac{Q^2 - m_t^2}{m_t^2} \right], \quad (2.7)$$

where  $R$  represents the cone size of the final state jet. Here the parameters  $A$ ,  $B$ ,  $D_1$  and  $D_2$  can be expanded perturbatively in  $\alpha_s$ , which is  $g_s^2/(4\pi)$ . At one-loop order,

$$A = C_F \frac{\alpha_s}{\pi}, \quad B = -2C_F \frac{\alpha_s}{\pi}, \quad D_1 = D_2 = C_F \frac{\alpha_s}{2\pi}, \quad (2.8)$$

with  $C_F = 4/3$ . In our numerical calculation, we will also include the  $A^{(2)}$  contribution, because it is associated with the incoming parton and is universal for all hard processes initiated by the same incoming parton [103],

$$A^{(2)} = C_F \left( \frac{\alpha_s}{\pi} \right)^2 \left[ \left( \frac{67}{36} - \frac{\pi^2}{12} C_A \right) - \frac{5}{18} N_f \right], \quad (2.9)$$

where  $C_A = 3$  and  $N_f = 5$  is the number of effective light quarks. The cone size  $R$  is introduced to regulate the collinear gluon radiation associated with the final state jet [73, 80–86].

The soft gluon radiation can be factorized out based on the Eikonal approximation method, i.e. for each incoming and outgoing color particles, the soft gluon radiation is factorized into an associated gauge link along the particle momentum direction. The color correlation between the color particles in this process is expanded by a group of orthogonal color bases. For the  $t$ -channel single top quark production, there are two orthogonal color configurations,

$$C_{1kl}^{ij} = \delta_{ik} \delta_{jl}, \quad C_{2kl}^{ij} = T_{ik}^{a'} T_{jl}^{a'}, \quad (2.10)$$

where  $i, j$  are color indices of the two incoming partons,  $k, l$  are color indices of the jet and the top quark in final states and  $a'$  is color index of the gluon. We follow the procedure of Ref. [82] to calculate the soft factor. Its definition in such color basis can be written as,

$$S_{IJ} = \int_0^\pi \frac{d\phi}{\pi} C_{I\bar{i}i'}^{bb'} C_{Jll'}^{aa'} \langle 0 | \mathcal{L}_{vcb'}^\dagger(b) \mathcal{L}_{\bar{v}bc'}(b) \mathcal{L}_{\bar{v}c'a'}^\dagger(0) \mathcal{L}_{vac}(0) \mathcal{L}_{n\bar{j}i}^\dagger(b) \mathcal{L}_{\bar{n}i'k}(b) \mathcal{L}_{\bar{n}kl}^\dagger(0) \mathcal{L}_{nl'j}(0) | 0 \rangle, \quad (2.11)$$

where we integrated out the azimuthal angle of the top quark and traded the relative azimuthal angle  $\phi$  for the  $q_\perp$ .  $I$  and  $J$  represent the color basis index,  $n$  and  $\bar{n}$  represent the momentum directions of the top quark and the jet in this process,  $v$  and  $\bar{v}$  are the momentum directions of the initial states. The gauge link  $\mathcal{L}_v(\xi)$  is defined along the  $v$  direction

$$\mathcal{L}_v(\xi) \equiv \text{Pexp} \left( -ig_s \int_{-\infty}^0 d\lambda v \cdot A(\lambda v + \xi) \right). \quad (2.12)$$

In this basis, the LO soft function is given by

$$\mathbf{S}^{(0)} = \begin{bmatrix} C_A^2 & 0 \\ 0 & \frac{C_A C_F}{2} \end{bmatrix}, \quad (2.13)$$

At the NLO level, the soft function can be represented as

$$\mathbf{S}^{(1)} = \sum_{i,j} \mathbf{W}_{ij} I_{ij}, \quad (2.14)$$

where  $\mathbf{W}_{ij}$  is the color matrix element. For subprocess  $ub \rightarrow dt$  [82]

$$\begin{aligned} W_{11} &= W_{22} = C_F \mathbf{S}^{(0)}, \\ W_{12} &= W_{34} = \begin{bmatrix} 0 & -\frac{C_A C_F}{2} \\ -\frac{C_A C_F}{2} & \frac{C_F^2}{2} \end{bmatrix} \\ W_{13} &= W_{24} = \begin{bmatrix} C_A^2 C_F & 0 \\ 0 & -\frac{C_F}{4} \end{bmatrix}, \\ W_{14} &= W_{23} = \begin{bmatrix} 0 & \frac{C_A C_F}{2} \\ \frac{C_A C_F}{2} & \frac{1}{4}(C_A^2 - 2)C_F \end{bmatrix}. \end{aligned} \quad (2.15)$$

For subprocess  $\bar{d}\bar{b} \rightarrow \bar{u}t$ ,

$$\begin{aligned} W_{11} &= W_{22} = C_F \mathbf{S}^{(0)}, \\ W_{12} &= W_{34} = \begin{bmatrix} 0 & \frac{C_A C_F}{2} \\ \frac{C_A C_F}{2} & \frac{1}{4}(C_A^2 - 2)C_F \end{bmatrix}, \\ W_{13} &= W_{24} = \begin{bmatrix} C_A^2 C_F & 0 \\ 0 & -\frac{C_F}{4} \end{bmatrix}, \\ W_{14} &= W_{23} = \begin{bmatrix} 0 & -\frac{C_A C_F}{2} \\ -\frac{C_A C_F}{2} & \frac{C_F^2}{2} \end{bmatrix}. \end{aligned} \quad (2.16)$$

$I_{ij}$  represents the kinematic integral for the soft gluon radiation between  $i$  and  $j$  gauge links,

$$I_{ij} = \frac{\alpha_s}{2\pi^2} \int_0^\pi \frac{(\sin \phi)^{-2\epsilon} d\phi}{\sqrt{\pi} \Gamma(1/2 - \epsilon)} \int dk^+ dk^- \frac{n_i \cdot n_j}{(k \cdot n_i)(k \cdot n_j)} \delta(k^2) \theta(k_0), \quad (2.17)$$

where  $k$  represents the radiated gluon momentum,  $n_{i,j}$  are dimensionless vectors along the directions of momentum  $p_{i,j}$ . The soft factor of the  $t$ -channel single top quark production

process at the NLO level is

$$\mathbf{S}^{(1)} = -\frac{\alpha_s}{2\pi} \mathbf{S}^{(0)} C_F \ln \frac{\mu^2 b_*^2}{b_0^2} \left[ -1 + \ln \left( \frac{\hat{s} - m_t^2}{R^2 P_{J\perp}^2} \frac{\hat{s} - m_t^2}{m_t^2} \right) \right] - \frac{\alpha_s}{2\pi} \left[ 2 \Xi \ln \frac{\mu^2 b_*^2}{b_0^2} + S^\epsilon \right], \quad (2.18)$$

where  $\Xi$  is process dependent, with

$$\Xi_{ub \rightarrow dt} = \frac{1}{2} \begin{bmatrix} 2C_F C_A^2 T & C_F C_A U \\ C_F C_A U & \frac{1}{2}(C_A^2 - 2)C_F U - \frac{C_F}{2} T \end{bmatrix}, \quad (2.19)$$

$$\Xi_{\bar{d}b \rightarrow \bar{u}t} = \frac{1}{2} \begin{bmatrix} 2C_F C_A^2 T & -C_F C_A U \\ -C_F C_A U & C_F U - \frac{C_F}{2} T \end{bmatrix}, \quad (2.20)$$

and

$$T = \ln\left(\frac{-\hat{t}}{\hat{s}}\right) + \ln\left(\frac{-(\hat{t} - m_t^2)}{\hat{s} - m_t^2}\right), \quad U = \ln\left(\frac{-\hat{u}}{\hat{s}}\right) + \ln\left(\frac{-(\hat{u} - m_t^2)}{\hat{s} - m_t^2}\right). \quad (2.21)$$

Here  $\hat{s} = x_1 x_2 S$ ,  $\hat{t} = (p_u - p_d)^2$ ,  $\hat{u} = (p_b - p_d)^2$  for the  $ub \rightarrow dt$  process, while for the  $\bar{d}b \rightarrow \bar{u}t$  process,  $\hat{t} = (p_{\bar{d}} - p_{\bar{u}})^2$  and  $\hat{u} = (p_b - p_{\bar{u}})^2$ . The matrix  $S^\epsilon$  is also process dependent,

$$S_{ub \rightarrow dt}^\epsilon = C_F \begin{bmatrix} C_A^2(I_S + I_L) & -(I_{3,4} - I_S) \frac{C_A}{2} \\ -(I_{3,4} - I_S) \frac{C_A}{2} & \frac{1}{2} I_{3,4} + \frac{(C_A^2 - 3)}{4} I_S + \frac{C_A C_F}{2} I_L \end{bmatrix}, \quad (2.22)$$

$$S_{\bar{d}b \rightarrow \bar{u}t}^\epsilon = C_F \begin{bmatrix} C_A^2(I_S + I_L) & (I_{3,4} - I_S) \frac{C_A}{2} \\ (I_{3,4} - I_S) \frac{C_A}{2} & \frac{(C_A^2 - 2)}{4} I_{3,4} + \frac{1}{4} I_S + \frac{C_A C_F}{2} I_L \end{bmatrix}, \quad (2.23)$$

where

$$I_L = \ln \frac{m_t^2}{m_t^2 + P_{J\perp}^2}, \quad I_S = \left[ \frac{1}{2} \ln^2 \left( \frac{1}{R^2} \right) - \text{Li}_2 \left( \frac{-P_{J\perp}^2}{m_t^2} \right) \right]. \quad (2.24)$$

The  $I_{3,4}$  represents the kinematic integral for the soft gluon radiation between the final state jet and top quark gauge links [88], and

$$\begin{aligned} I_{3,4} = & -\text{Li}_2 \frac{m_t^2 + \hat{t} - \hat{u}}{\hat{t}} - \text{Li}_2 \frac{(2m_t^2 - \hat{s})(m_t^2 - \hat{t})}{\hat{s}\hat{t}} + \text{Li}_2 \frac{(\hat{s} - 2m_t^2)\hat{t}}{\hat{s}\hat{u}} - \ln \frac{m_t^2 - \hat{u}}{m_t^2 + \hat{t} - \hat{u}} \ln \frac{-m_t^2(m_t^2 + \hat{t} - \hat{u})}{\hat{s}\hat{u}} \\ & + \ln \frac{-\hat{t}}{m_t^2 + \hat{t} - \hat{u}} \ln \frac{(m_t^2 - \hat{s})(m_t^2 + \hat{t} - \hat{u})}{\hat{s}\hat{u}} + (\hat{t} \leftrightarrow \hat{u}) - \ln \frac{\hat{s} - m_t^2}{m_t^2} \ln \frac{\hat{t}\hat{u}}{m_t^4 - (\hat{t} - \hat{u})^2} \\ & - \ln \frac{P_{J\perp}^2 R^2 \hat{s}}{\hat{t}\hat{u}} \ln \frac{\hat{s} - m_t^2}{-P_{J\perp}^2 R^2} - \frac{1}{2} \ln^2 \frac{P_{J\perp}^2 R^2}{\hat{s} - 2m_t^2} - \frac{1}{2} \ln^2 \frac{m_t^2}{2m_t^2 - \hat{s}} + \frac{1}{2} \ln^2 \frac{\hat{s} - m_t^2}{2m_t^2 - \hat{s}} - \ln \frac{\hat{s} - m_t^2}{2m_t^2 - \hat{s}} \ln \frac{P_{J\perp}^2 R^2}{\hat{s} - 2m_t^2} \\ & + 2 \ln \frac{\hat{s} - m_t^2}{2m_t^2 - \hat{s}} \ln \frac{P_{J\perp}^2 R^2}{\hat{s} - m_t^2} + \ln \frac{m_t^2}{2m_t^2 - \hat{s}} \ln \frac{m_t^2 \hat{s}}{\hat{t}\hat{u}} - 2 \ln \frac{2m_t^2 - \hat{s}}{m_t^2 - \hat{s}} \ln \frac{m_t^2}{2m_t^2 - \hat{s}} - 2 \text{Li}_2 \frac{m_t^2}{\hat{s} - m_t^2} - \frac{\pi^2}{3}. \end{aligned} \quad (2.25)$$

In the massless limit of the top quark, it will recover the result of dijet production, as in Ref. [82],

$$I_{3,4} = \frac{1}{2} \ln^2 \frac{1}{R_1^2} + \frac{1}{2} \ln^2 \frac{1}{R_2^2} + \frac{\pi^2}{3} - 4 \ln \frac{-\hat{s}}{\hat{t}} \ln \frac{-\hat{s}}{\hat{u}}, \quad (2.26)$$

where  $R_1$  and  $R_2$  are the radii of the two cone jets.

$S_{IJ}$  satisfies the renormalization group equation,

$$\frac{d}{d \ln \mu} S_{IJ}(\mu) = - \sum_L S_{IL} \Gamma_{LJ}^S - \sum_L \Gamma_{IL}^{S\dagger} S_{LJ}, \quad (2.27)$$

where

$$\mathbf{\Gamma}^S = \frac{\alpha_s}{2\pi} \left[ -1 + \ln \frac{\hat{s} - m_t^2}{R^2 P_{J\perp}^2} + \ln \frac{\hat{s} - m_t^2}{m_t^2} \right] C_F \mathbf{\Gamma}^E + \gamma^S. \quad (2.28)$$

Here  $\mathbf{\Gamma}^E$  is an identity matrix and  $\gamma^S$  is the associated anomalous dimension. We obtain

$$\begin{aligned} \gamma^S_{ub \rightarrow dt} &= \frac{\alpha_s}{\pi} \begin{bmatrix} C_F T & C_F/C_A U \\ U & \frac{1}{2}(C_A - 2/C_A)U - \frac{1}{2C_A} T \end{bmatrix}, \\ \gamma^S_{\bar{d}b \rightarrow \bar{u}t} &= \frac{\alpha_s}{\pi} \begin{bmatrix} C_F T & -\frac{C_F}{2C_A} U \\ -U & -\frac{1}{2C_A}(T - 2U) \end{bmatrix}. \end{aligned} \quad (2.29)$$

The jet function originated from the collinear gluon radiation of jet . In this work, we apply the anti- $k_T$  jet algorithm as in Refs. [82, 104], and

$$J_q = \frac{\alpha_s C_F}{2\pi \Gamma(1-\epsilon)} \left[ \frac{1}{\epsilon^2} + \frac{1}{\epsilon} \left( \frac{3}{2} - \ln \frac{P_{J\perp}^2 R^2}{\mu_{\text{Res}}^2} \right) + I_q \right], \quad (2.30)$$

where  $\epsilon = (D-4)/2$  in D-dimensional regularization, and the finite term  $I_q$  is

$$I_q = \frac{1}{2} \left( \ln \frac{P_{J\perp}^2 R^2}{\mu_{\text{Res}}^2} \right)^2 - \frac{3}{2} \ln \frac{P_{J\perp}^2 R^2}{\mu_{\text{Res}}^2} + \frac{13}{2} - \frac{2}{3} \pi^2. \quad (2.31)$$

The singular terms in the jet function are independent of jet algorithm, while the finite term  $I_q$  depends on the jet clustering algorithm. The contribution from the jet function is proportional to the leading order cross section and has been included in the following hard matrix  $\mathbf{H}$ .

The hard matrix in the color basis of Eq. (2.10) can be expressed as

$$\mathbf{H} = \begin{bmatrix} H^{(0)} + H^{(1)} & H_{12}^{(1)} \\ H_{12}^{(1)} & 0 \end{bmatrix}, \quad (2.32)$$

where  $H^{(0)}$  denotes the leading order hard matrix element, which is given as

$$H^{(0)}(ub \rightarrow dt) = \frac{1}{C_A^2} \frac{g^4 \hat{s}(\hat{s} - m_t^2)}{4(\hat{t} - m_W^2)^2} |V_{ud}|^2 |V_{tb}|^2, \quad (2.33)$$



with  $g$  being the  $SU(2)_L$  gauge coupling. The CKM matrix element  $V_{ij}$  needs to change in accordance with the quark flavors of the hard scattering process.  $m_W$  is the  $W$ -boson mass. The spin and color average factors have been included. Another  $t$ -channel matrix element  $H^{(0)}(\bar{u}b \rightarrow \bar{d}t)$  can be obtained by exchange  $\hat{s}$  to  $\hat{u}$ . The hard matrix elements  $H^{(1)}$  and  $H_{12}^{(1)}$  are from one-loop QCD correction. The numerical result shows that the contribution from  $H_{12}^{(1)}$  can be ignored and the analytical result can be obtained from Eq. (A.7) of Ref. [69] by crossing symmetry (by exchanging  $\hat{s} \leftrightarrow \hat{t}$  for  $ub \rightarrow dt$  production process), thus we only show the diagonal element  $H^{(1)}$  as below.

$$\begin{aligned}
H^{(1)} = & \frac{\alpha_s}{2\pi} H^{(0)} \left[ -\ln^2(1-\lambda) - \frac{\ln(1-\lambda)}{\lambda} - 2\ln(1-\lambda) - 2\ln(1-\lambda) \ln \frac{\hat{s}}{m_t^2} \right. \\
& + \ln \frac{\mu_{\text{Res}}^2}{\hat{s}} \left( -2\ln(1-\lambda) - \ln \frac{\hat{s}}{m_t^2} - 2\ln \frac{-\hat{s}}{\hat{t}} - \frac{11}{2} \right) - \frac{1}{2} \ln^2 \frac{\hat{s}}{m_t^2} - \frac{5}{2} \ln \frac{\hat{s}}{m_t^2} - \frac{3}{2} \ln \frac{P_{J\perp}^2 R^2}{\mu_{\text{Res}}^2} \\
& \left. + 2\text{Li}_2(\lambda) + \frac{1}{2} \ln^2 \frac{P_{J\perp}^2 R^2}{\mu_{\text{Res}}^2} - \frac{3}{2} \ln^2 \frac{\mu_{\text{Res}}^2}{\hat{s}} - \ln^2 \frac{-\hat{s}}{\hat{t}} - 3\ln \frac{-\hat{s}}{\hat{t}} - \frac{5\pi^2}{6} - \frac{15}{2} \right] + \delta H^{(1)},
\end{aligned} \tag{2.34}$$

where  $\lambda = \hat{t}/(\hat{t} - m_t^2)$ , and the  $\delta H^{(1)}$  is not proportional to the leading order cross section,

$$\delta H^{(1)} = \frac{\alpha_s}{2\pi} \frac{1}{4C_A^2} \frac{g^4 C_F m_t^2}{(\hat{t} - m_W^2)^2} \frac{\hat{s}\hat{u}}{\hat{t}} \ln \frac{m_t^2}{m_t^2 - \hat{t}} |V_{ud}|^2 |V_{tb}|^2, \tag{2.35}$$

where the spin and color average factors have also been included.

We should note that the non-global logarithms (NGLs) could also contribute to this process. The NGLs arise from some special kinematics of two soft gluon radiations, in which the first one is radiated outside of the jet which subsequently radiates a second gluon into the jet [105–108]. Numerically, the NGLs are negligible in this process since it starts at  $\mathcal{O}(\alpha_s^2)$ . Therefore we will ignore their contributions in the following phenomenology discussion.

### 3 Phenomenology

Below, we present the numerical result of resummation calculation for the  $t$ -channel single top (anti-) quark production at the  $\sqrt{S} = 13$  TeV LHC with CT14NNLO PDF [95]. Figure 1 shows the  $q_\perp$  distribution from the asymptotic piece (blue dashed line), NLO calculation (red dotted line), resummation prediction (black solid line) and  $Y$ -term (orange dot-dashed line) for the top quark (a, b) and the anti-top quark (c, d) production. Here, the asymptotic piece is the fixed-order expansion of Eq. (2.1) up to the  $\alpha_s$  order, and is expected to agree with the NLO prediction as  $q_\perp \rightarrow 0$ . In the same figure, we also compare to the prediction from the parton shower event generator PYTHIA 8 [109] (green solid line), which was calculated at the leading order, with CT14LO PDF. For the fixed-order calculation, both the renormalization and factorization scales are fixed at  $H_T \equiv \sqrt{m_t^2 + P_{J\perp}^2} + P_{J\perp}$ . Similarly, in the resummation calculation, the canonical choice of the resummation ( $\mu_{\text{Res}}$ ) and renormalization ( $\mu_{\text{ren}}$ ) scales is

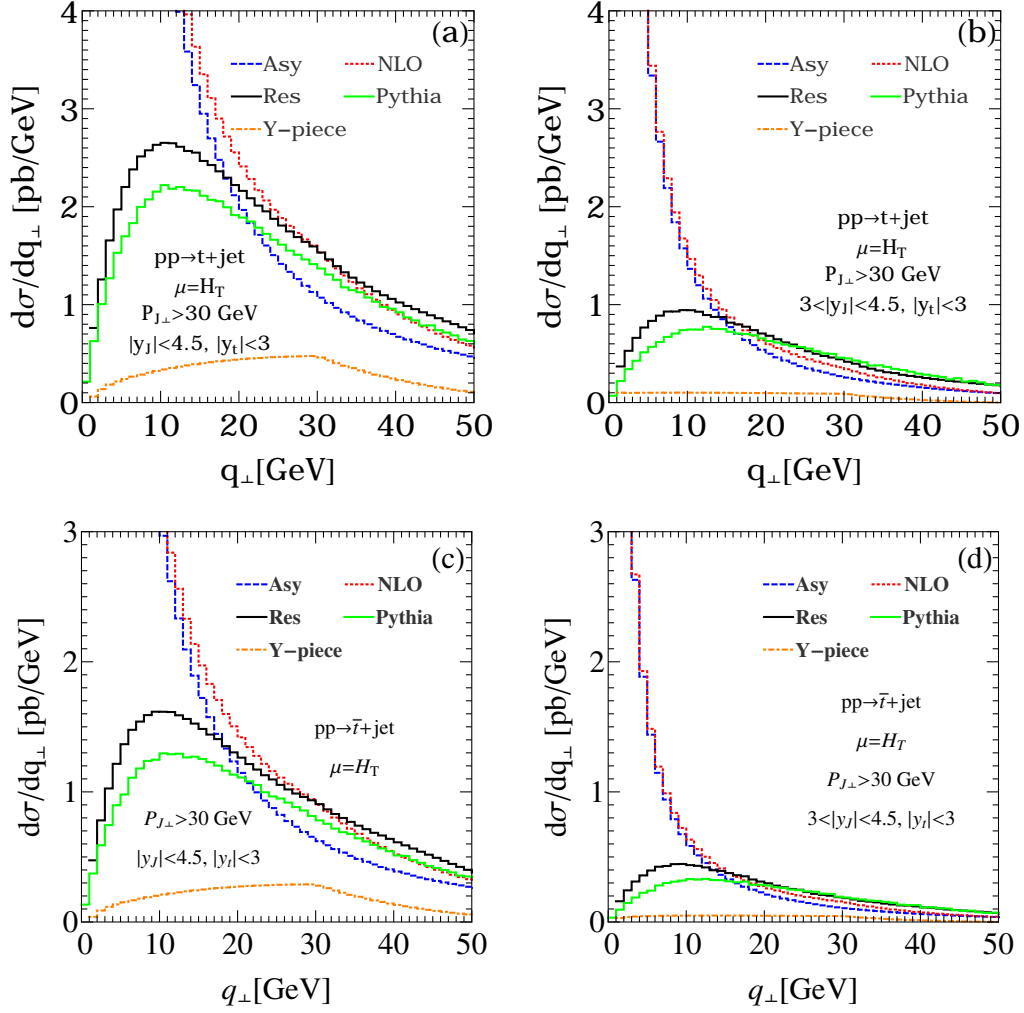


**Figure 1.** The  $q_{\perp}$  distribution from the asymptotic result (blue dashed line), NLO calculation (red dotted line), resummation prediction (black solid line), parton shower result by PYTHIA 8 (green solid line) and  $Y$ -term (orange dot-dashed line) for the  $t$ -channel single top quark production (a, b) and the anti-top quark production (c, d) at the  $\sqrt{S} = 13$  TeV LHC with  $|y_t| < 3$  and  $|y_J| \leq 4.5$  (a, c), or  $3.0 \leq |y_J| \leq 4.5$  (b, d). The resummation and renormalization scales are choose as  $\mu = \mu_{\text{Res}} = \mu_{\text{ren}} = H_T$ .

taken to be  $H_T$  in this study. The uncertainties of the resummation predictions are estimated by varying the scale  $\mu_{\text{Res}} = \mu_{\text{ren}}$  by a factor two around the central value  $H_T$ , which is shown in Fig. 2. The jet cone size is choose as  $R = 0.4$ , using the anti- $k_T$  algorithm, and the Wolfenstein CKM matrix elements parameterization is used in our numerical calculation [110]. We shall compare predictions for two different sets of kinematic cuts, with  $|y_t| \leq 3$  and  $P_{J\perp} > 30$  GeV, and  $|y_J| \leq 4.5$  in (a, c), and  $3 \leq |y_J| \leq 4.5$  in (b, d) of Fig. 1, respectively. Some results of the comparison are in order. Clearly, the asymptotic piece and the fixed-order

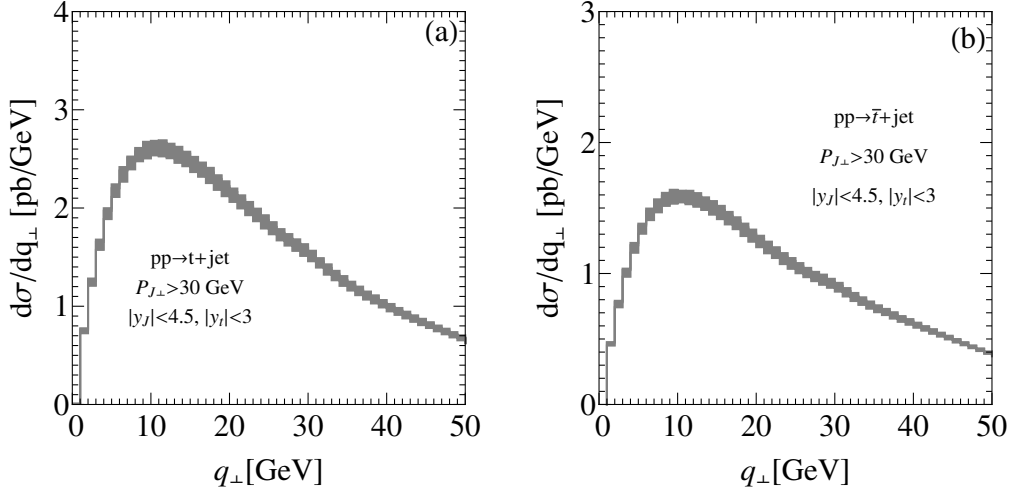


**Figure 2.** The scale uncertainties for the  $t$ -channel single top quark production (a) and the anti-top quark production (b) at the  $\sqrt{S} = 13$  TeV LHC with  $|y_t| < 3$ ,  $|y_J| \leq 4.5$  and  $P_{J\perp} > 30$  GeV. The resummation and renormalization scales are varied from  $H_T/2$  to  $2H_T$ .

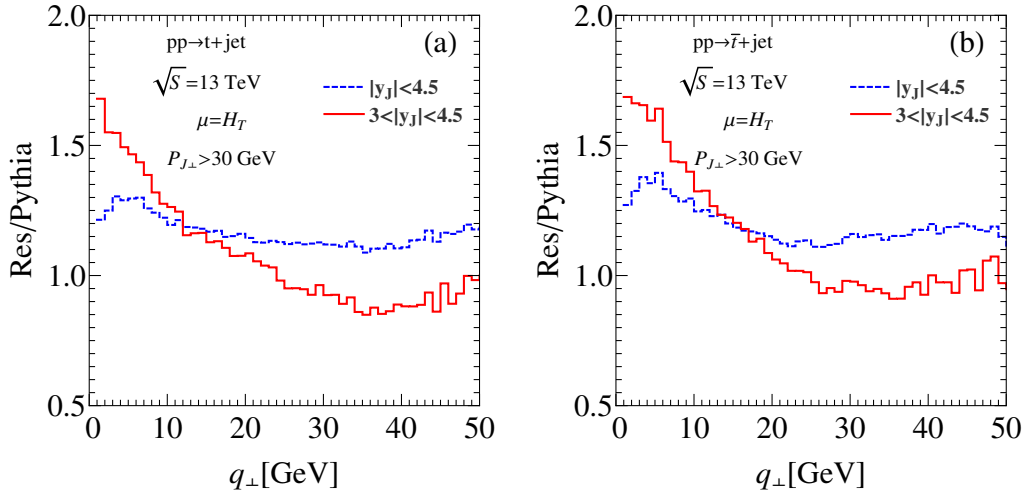


**Figure 3.** The ratio of the resummation and PYTHIA prediction for the  $t$ -channel single top quark production (a) and anti-top quark production (b) at the  $\sqrt{S} = 13$  TeV LHC with  $|y_t| < 3$ ,  $P_{J\perp} > 30$  GeV and  $|y_J| \leq 4.5$  (blue dashed line), or  $3.0 \leq |y_J| \leq 4.5$  (red solid line). The resummation and renormalization scales are choose as  $\mu = \mu_{\text{Res}} = \mu_{\text{ren}} = H_T$ .

calculation results agree very well in the small  $q_\perp$  (less than 1 GeV) region. As a further check of our resummation calculation, we integrate out the  $q_\perp$  distribution to compare the total cross section with that predicted by the NLO program MCFM [111]. In the resummation framework, the NLO total cross section can be divided into two parts, the small  $q_\perp$  region, which can be obtained by integrating the distribution of the asymptotic part and the one-

loop virtual diagram contribution, and the large  $q_\perp$  part, which is infrared safe and can be numerically calculated directly. Thus, the total cross section is given by

$$\sigma_{NLO} = \int_0^{q_{\perp,0}^2} dq_\perp^2 \frac{d\sigma_{NLO}^{virtual+real}}{dq_\perp^2} + \int_{q_{\perp,0}^2}^\infty dq_\perp^2 \frac{d\sigma_{NLO}^{real}}{dq_\perp^2}. \quad (3.1)$$

It is obvious that the two contributions on the right-hand side of the above equation depend on the cut-off parameter  $q_{\perp,0}$  individually, but their sum is independent of it. We show the total NLO cross section of  $pp \rightarrow t(\bar{t}) + jets$  as a function of  $q_{\perp,0}$ , in Fig. 4. It is clear that the total cross sections of top quark and anti-top quark do not depend on  $q_{\perp,0}$ , which varies from 0.1 GeV to 1.5 GeV. We also checked that the total cross sections from our resummation and MCFM calculations are in perfect agreement.

As shown in Fig. 1, the NLO prediction is not reliable when the  $q_\perp$  is small. The resummation calculation predicts a well behaved  $q_\perp$  distribution in the small  $q_\perp$  region since the large logarithms have been properly resummed. In Fig 3, we compare the predictions from our resummation calculation to PYTHIA by taking the ratio of their  $q_\perp$  differential distributions shown in Fig. 1. With the jet rapidity  $|y_J| \leq 4.5$  (blue solid line), its ratio is not sensitive to  $q_\perp$ , for either single top (a) or anti-top quark (b) production. Hence, they predict almost the same shape in  $q_\perp$  distribution, while they predict different fiducial total cross sections because PYTHIA prediction includes only leading order matrix element and is calculated with CT14LO PDFs. However, if we require the final state jet to be in the forward rapidity region, with  $3 \leq |y_J| \leq 4.5$  (red solid line), which is the so-called signal region of single top events [42], we find that PYTHIA prediction disagrees with our resummation calculation. Our resummation calculation predicts a smaller  $q_\perp$  value when the final state jet is required to fall into the forward region, i.e., the signal region. We have checked that the PYTHIA result is not sensitive to the effects from beam remnants. Furthermore, the  $Y$ -term contribution, from NLO, is negligible in this region, cf. Fig. 1(b) and (d) (orange dot-dashed line). Hence, we conclude that their difference most likely comes from the treatment of multiple soft gluon radiation.

As shown in Eqs. (2.18)-(2.21), the effect of multiple gluon radiation, originated from soft gluons connecting the initial and final state gauge links, becomes more important when the final state jet is required to be in the forward region where the kinematic factor  $T \sim \ln \frac{-\hat{t}}{\hat{s}}$  becomes large as  $|\hat{t}| \rightarrow 0$ . Consequently, the  $q_\perp$  distribution peaks at a smaller value as compared to the case in which the final state jet does not go into the forward region. To illustrate this, we compare in Fig. 5 the predictions of the  $W$ -term in our resummation calculation, cf. the first term of Eq. (2.1), with or without including the factor  $T$  in Eqs. (2.18)-(2.21), which arises from the soft gluon interaction between the initial and final states gauge links. The comparison was made for single top (a) and single anti-top (b) quark production with two different  $|y_J|$  regions. It clearly shows that the color coherence effect between the

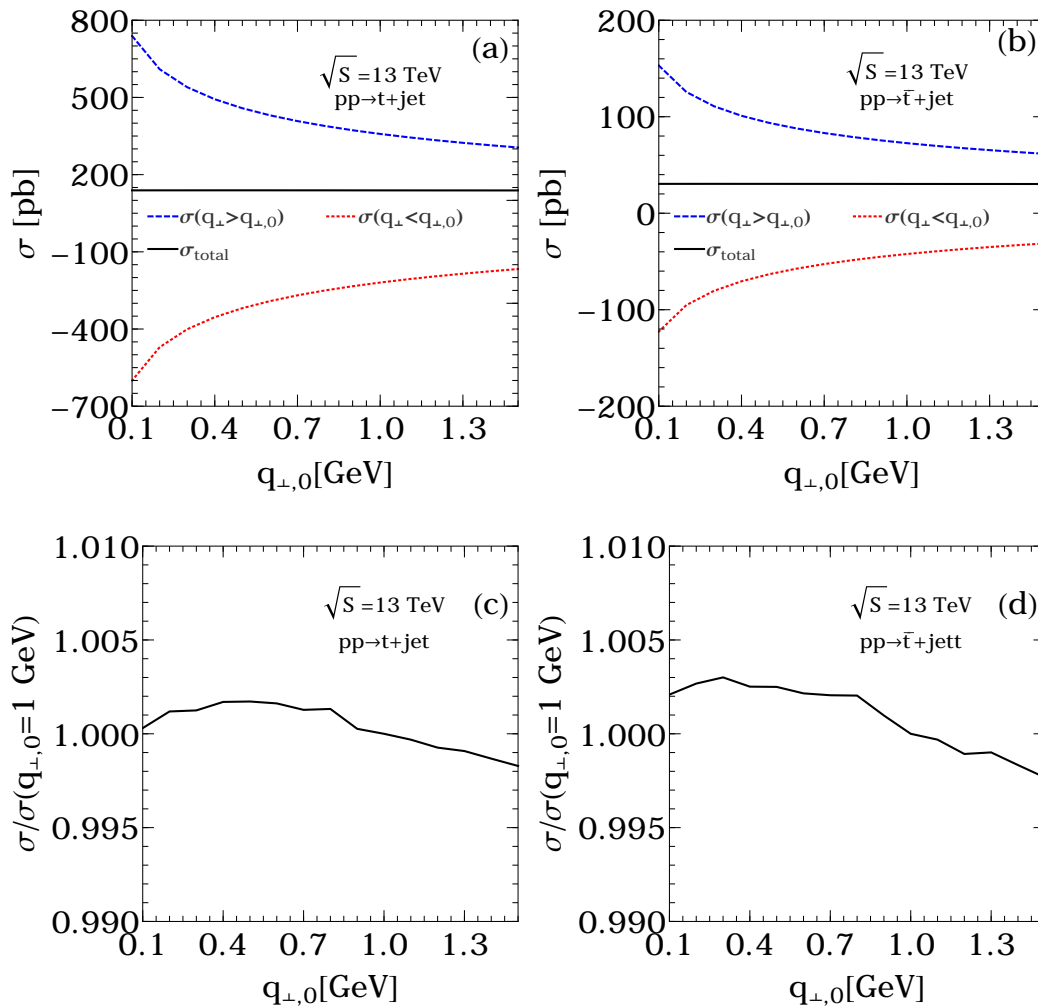


**Figure 4.** The upper blue dashed curve shows the contribution from the second term of the right-hand side of Eq. (3.1), the lower red dotted curve from the first term, and the black solid line shows the total cross section, at the NLO (a, b). The ratio plots  $\sigma/\sigma(q_{\perp,0} = 1 \text{ GeV})$  are shown in (c, d).

initial and final state colored particles pushes  $q_{\perp}$  to a smaller value. Such effects become more important when the final state jet is required to be in the forward region ( $3 \leq |y_J| \leq 4.5$ ).

Next, we examine the effect of the incoming bottom quark mass to the  $q_{\perp}$  distribution. To be consistent with the (CT14) PDFs which were determined using the S-ACOT scheme to define heavy parton, Eq. (2.5) is used in the calculation of the  $W$ -piece. In the limit of  $m_b \rightarrow 0$ , it reduces to the usual Wilson coefficient [100–102] (see Eq. (2.6)). As shown in Fig. 6, the correct treatment of the finite bottom quark mass, with  $m_b = 4.75 \text{ GeV}$ , shifts the peak of the  $q_{\perp}$  distribution by about  $3 \sim 4 \text{ GeV}$  as compared to massless case.

It is also desirable to compare the rapidity distribution of the final state jet in various calculations. Figure 7 shows the jet rapidity distributions predicted by our resummation

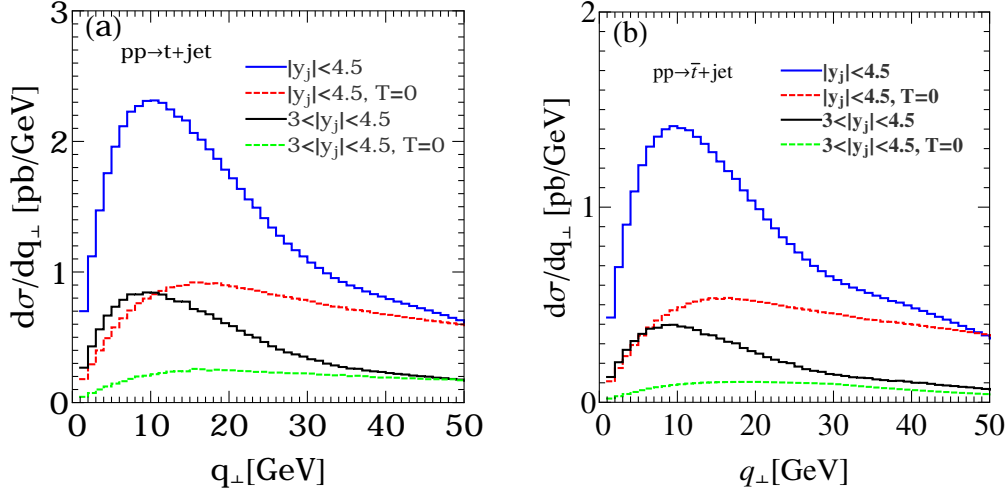


**Figure 5.** (a) The  $W$ -piece prediction for the  $t$ -channel single top quark production (a) and anti-top quark production (b) at the  $\sqrt{S} = 13$  TeV LHC with  $|y_t| < 3$  and  $P_{J\perp} > 30$  GeV. The blue solid and red dashed line represents the prediction with and without including the factor  $T$  in Eqs. (2.18)-(2.21) with  $|y_J| \leq 4.5$ , respectively, black solid and green dashed lines are for the  $3 \leq |y_J| \leq 4.5$ . The resummation and renormalization scales are choose as  $\mu = \mu_{\text{Res}} = \mu_{\text{ren}} = H_T$ .

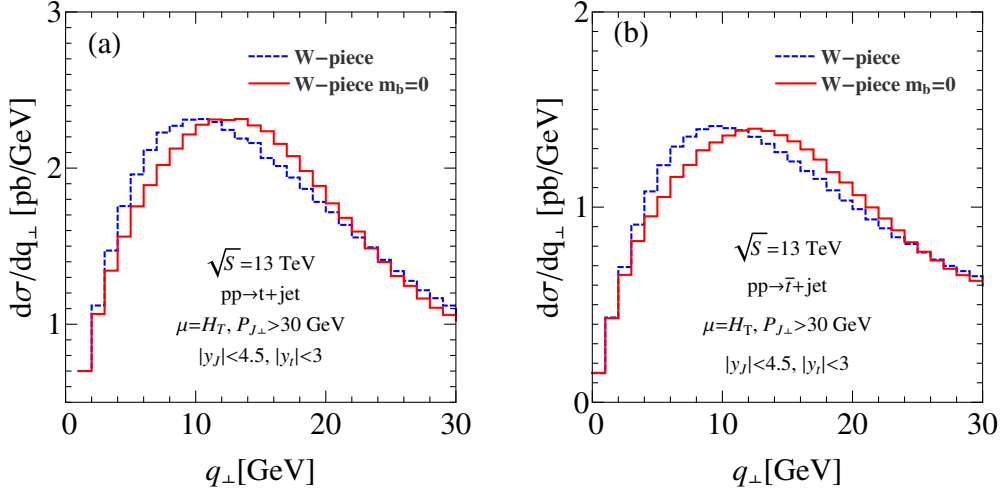


**Figure 6.** The  $W$ -piece prediction for the single top quark production (a) and anti-top quark production (b) with non-zero  $m_b$  (blue dashed line) and  $m_b = 0$  (red solid line) at the  $\sqrt{S} = 13$  TeV LHC with  $|y_J| \leq 4.5$ ,  $|y_t| < 3$  and  $P_{J\perp} > 30$  GeV. The resummation and renormalization scales are choose as  $\mu = \mu_{\text{Res}} = \mu_{\text{ren}} = H_T$ .

calculation (blue solid line), NLO (red dashed line), PYTHIA (green solid line), and LO calculation with CT14LO PDF (black dotted line), at the  $\sqrt{S} = 13$  TeV LHC, with  $|y_t| < 3$  and  $P_{J\perp} > 30$  GeV. For this comparison, both the renormalization and factorization

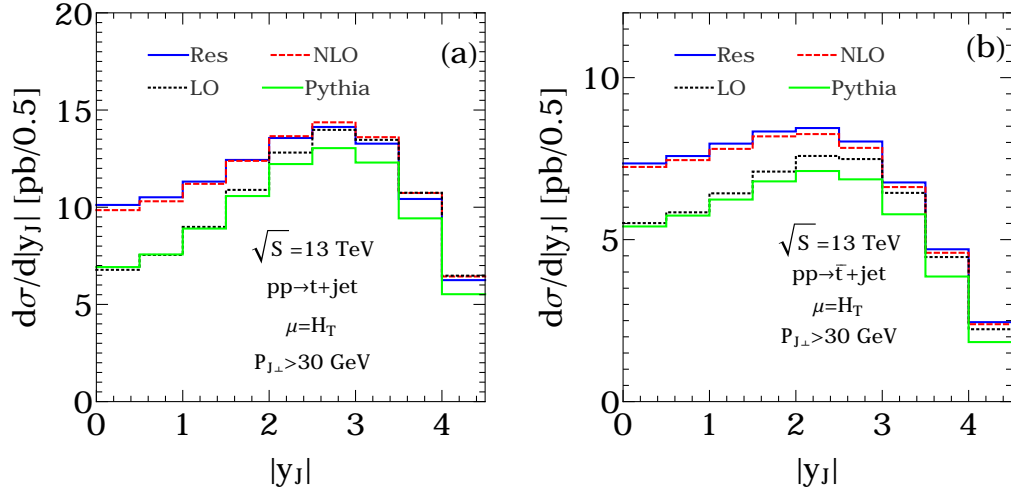


**Figure 7.** (a) The jet rapidity distribution for the  $t$ -channel single top quark production (a) and anti-top quark production (b) from resummation prediction (blue solid line), NLO results (red dashed line), LO calculation with CT14LO PDF (black dashed line) and PYTHIA prediction (green solid line) at the  $\sqrt{S} = 13$  TeV LHC with  $|y_t| < 3$  and  $P_{J\perp} > 30$  GeV. The renormalization and factorization scales are choose as  $\mu = \mu_{\text{ren}} = \mu_F = H_T$  in the fixed-order calculation.

**Table 1.** The predicted kinematic acceptances for the  $\phi^*$  cut-off in the  $t$ -channel single top quark production at the LHC

$\phi^*(t)$		< 0.05	< 0.1	< 0.15	< 0.2	< 0.25	< 0.3
Res	$ y_J  < 4.5$	48%	68 %	79%	86%	91%	94%
PYTHIA	$ y_J  < 4.5$	46%	68%	81%	88%	93%	96%
Res	$3 <  y_J  < 4.5$	54%	72%	83%	89%	93%	96%
PYTHIA	$3 <  y_J  < 4.5$	46%	68%	80%	87%	92%	96%
$\phi^*(\bar{t})$		< 0.05	< 0.1	< 0.15	< 0.2	< 0.25	< 0.3
Res	$ y_J  < 4.5$	48%	68%	79%	86%	90%	94 %
PYTHIA	$ y_J  < 4.5$	48%	70%	82%	89%	93%	96%
Res	$3 <  y_J  < 4.5$	54%	72%	82%	88%	92%	95%
PYTHIA	$3 <  y_J  < 4.5$	48%	69%	81%	88%	93%	96%

scales are fixed at  $H_T$  in the fixed-order calculation, while  $\mu_{\text{Res}} = H_T$  and  $\mu_F = b_0/b_*$  in the resummation calculation. Firstly, we note that the NLO QCD correction modifies the shapes of the  $y_J$  with respect to PYTHIA prediction which is based on the leading order matrix element calculation. The similar result was discussed in Ref. [48]. This is due to the sizeable NLO corrections originated from gluon scattering sub-processes which generate a large correction to the central jet rapidity region and result in different shape between the NLO and LO results. Secondly, the differential cross section predicted by the resummation

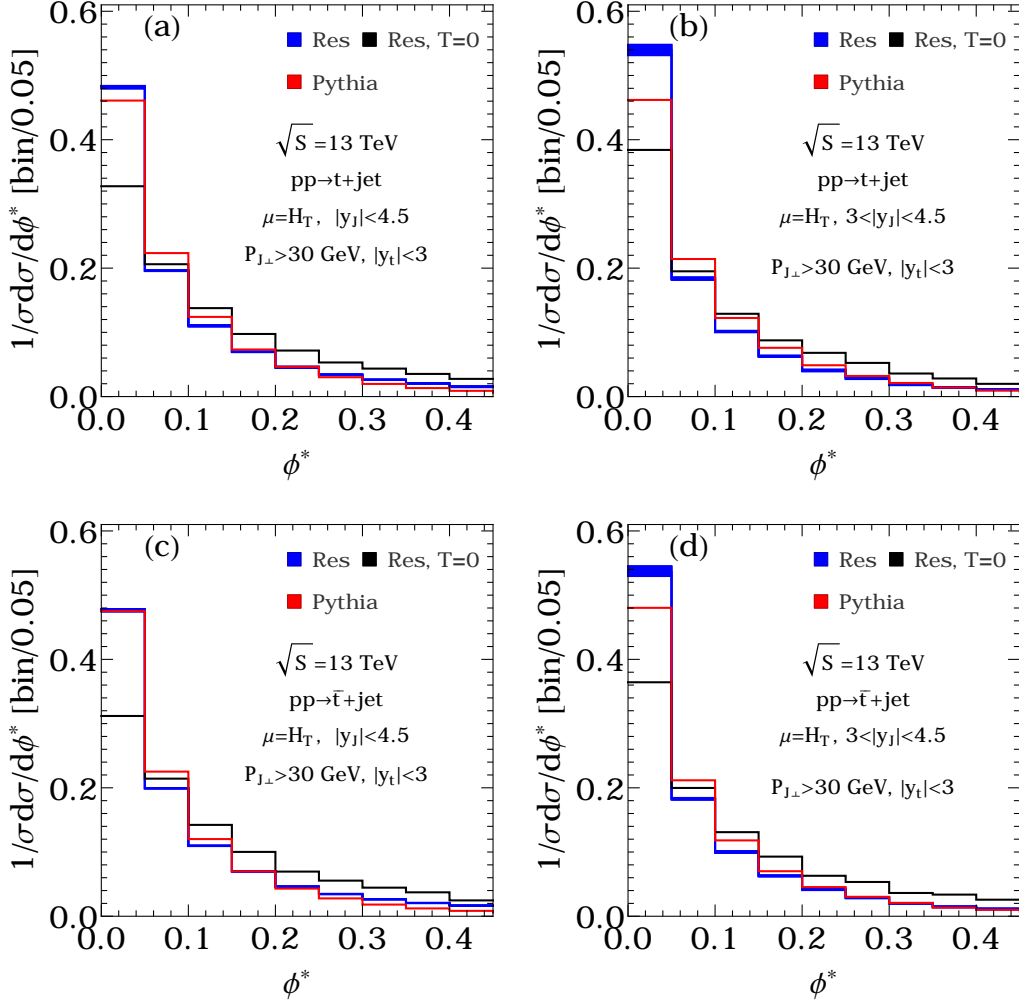


**Figure 8.** The normalized distribution of  $\phi^*$  for top quark production at the  $\sqrt{S} = 13$  TeV LHC with  $|y_t| < 3$  and  $P_{J\perp} > 30$  GeV. The resummation and renormalization scales are choose as  $\mu = \mu_{\text{Res}} = \mu_{\text{ren}} = H_T$ . The blue and black line represents the resummation prediction with and without including the factor  $T$  in Eqs. (2.18)-(2.21), respectively. The red lines describe the results from PYTHIA prediction. The blue shaded region represents the scale uncertainties which are varied from  $H_T/2$  to  $2H_T$ .

calculation is about the same as the NLO prediction.

As discussed above, the coherence effect of gluon radiation in the initial and final states becomes large when the final state jet falls into more forward (or backward) direction, with a larger absolute value of pseudorapidity. Furthermore, a different prediction in  $q_\perp$  would lead to different prediction in the azimuthal angle between the final state jet and the top quark moving directions measured in the laboratory frame. Both of them suggest that we could use the well-known  $\phi^*$  distribution, for describing the precision Drell-Yan pair kinematical



distributions [112], to test the effect of multiple gluon radiation in the  $t$ -channel single top (anti-) quark production. The advantage of studying the  $\phi^*$  distribution is that it only depends on the moving directions (not energies) of the final state jet and top (anti-) quark. Hence, it might provide a more sensitive experimental observable when the final state jet falls into forward (or backward) direction. We follow its usual definition and define

$$\phi^* = \tan\left(\frac{\pi - \Delta\phi}{2}\right) \sin\theta_\eta^*, \quad (3.2)$$

where  $\Delta\phi$  is the azimuthal angle separation in radians between the jet and top quark. The angle  $\theta_\eta^*$  is defined as,

$$\cos\theta_\eta^* = \tanh\left[\frac{\eta_J - \eta_t}{2}\right], \quad (3.3)$$

where  $\eta_J$  and  $\eta_t$  are the pseudorapidities of the jet and top quark, respectively. Here, we used pseudorapidity, instead of rapidity, of top quark because rapidity depends on the energy of particle.

As shown in Fig. 8, the predictions of PYTHIA and our resummation calculation differ in the small  $\phi^*$  region, especially for the final state jet falls into more forward (or backward) direction (Fig. 8(b, d)), which can be caused by a large value of  $\eta_J - \eta_t$ . i.e., in the events with large rapidity gap. In such region, the subleading logarithm terms in the Sudakov factor are important in our resummation calculation. To illustrate this, we also compare to the prediction (shown as black curves in Fig. 8) without the coherence factor  $T$  in Eqs. (2.18)-(2.21). It shows that factor  $T$  would change  $\phi^*$  distribution significantly.

Since  $\phi^*$  is sensitive to the color structure of the signal, it could also be used to improve the  $t$ -channel single top quark cross section measurement. In that case, a precise theoretical evaluation of the kinematic acceptance after imposing the kinematic cuts is necessary, which is defined as,

$$\epsilon \equiv \frac{\sigma(\phi^* < \phi^0)}{\sigma}. \quad (3.4)$$

Here,  $\sigma(\phi^* < \phi^0)$  is the cross section after imposing the kinematic cuts, while  $\sigma$  is not. As shown in Table 1, if we require the final state jet to be in the forward rapidity region, with  $3 \leq |y_J| \leq 4.5$ , the kinematic acceptance with  $\phi^* < 0.05$  is larger by about 15% for top quark and 11% for anti-top quark in our resummation calculation than the PYTHIA prediction. For  $\phi^* < 0.1$ , they differ by about 6% for top quark and 4% for anti-top quark, and our resummation calculation predicts a larger total fiducial cross section. Currently, the ATLAS and CMS Collaborations have measured the  $t$ -channel single top quark at the 13 TeV LHC, the uncertainty is around 10% [44, 113]. If the  $\phi^*$  observable is used to further suppress backgrounds and enhance the signal to backgrounds ratio, the difference found in our resummation and PYTHIA calculations of the fiducial cross section could become important. This will lead to, for example, different conclusion about the constraints on various  $Wtb$  anomalous couplings, induced by New Physics, or the measurement of  $V_{tb}$  [12, 19].

## 4 Conclusions

In this paper, we studied the  $q_\perp$  resummation effects for the  $t$ -channel single top quark production at the LHC based on the TMD factorization theorem. The large logarithm  $\ln(Q^2/q_\perp^2)$  was resummed by renormalization group evolution. In order to validate our resummation formula, we expand it to the NLO to obtain the singular terms and compare the transverse momentum distributions at the NLO level. It shows perfect agreement in the small  $q_\perp$  region. We also calculate the NLO total cross section based on the resummation framework, and our results are in perfect agreement with MCFM.

We then perform the calculation of the  $q_\perp$  distribution at NLL accuracy, and compare them with predictions from PYTHIA. It shows that the Sudakov peak in this process is sensitive to the soft gluon interaction between the initial and final states, and the bottom quark mass. Furthermore, we find the shape of  $q_\perp$  spectrum from the our resummation calculation agrees well with PYTHIA results when the final state jet is allowed to fall into the full rapidity region, but there is a large deviation when the final state jet is required to be in the forward (or backward) region. The rapidity distribution of the final state jet in various calculation are also discussed. We note that the NLO QCD correction modifies the shapes of the  $y_J$  with respect to the PYTHIA and LO predictions, and the resummation calculation presented in this work is at the NLO-NLL accuracy.

Finally, we propose to measure the experimental observable  $\phi^*$ , similar the one used in analyzing the precision Drell-Yan data, to perform precision test of the SM in the production of the  $t$ -channel single top events at the LHC. It shows the predictions of PYTHIA and our resummation calculation differ in the small  $\phi^*$  region, especially when the final state jet falls into more forward (or backward) region. The difference found in our resummation and PYTHIA calculations of the fiducial cross section could become important if  $\phi^*$  is used to further suppress the backgrounds in order to determine the CKM mixing-matrix element  $V_{tb}$  or to probe new physics effect through measuring the  $Wtb$  couplings in the  $t$ -channel single-top events produced at hadron colliders.

## Acknowledgments

This work is partially supported by the U.S. Department of Energy, Office of Science, Office of Nuclear Physics, under contract number DE-AC02-05CH11231; by the U.S. National Science Foundation under Grant No. PHY-1719914; and by the National Natural Science Foundation of China under Grant Nos. 11275009, 11675002, 11635001 and 11725520. C.-P. Yuan is also grateful for the support from the Wu-Ki Tung endowed chair in particle physics.

## References

- [1] S. Dawson, Nucl. Phys. **B249**, 42 (1985).
- [2] S. S. D. Willenbrock and D. A. Dicus, Phys. Rev. **D34**, 155 (1986).

- [3] S. Dawson and S. S. D. Willenbrock, Nucl. Phys. **B284**, 449 (1987).
- [4] C. P. Yuan, Phys. Rev. **D41**, 42 (1990).
- [5] G. L. Kane, G. A. Ladinsky, and C. P. Yuan, Phys. Rev. **D45**, 124 (1992).
- [6] D. O. Carlson, E. Malkawi, and C. P. Yuan, Phys. Lett. **B337**, 145 (1994), [hep-ph/9405277](#).
- [7] C.-R. Chen, F. Larios, and C. P. Yuan, Phys. Lett. **B631**, 126 (2005), [hep-ph/0503040](#).
- [8] Q.-H. Cao, J. Wudka, and C. P. Yuan, Phys. Lett. **B658**, 50 (2007), [0704.2809](#).
- [9] E. L. Berger, Q.-H. Cao, and I. Low, Phys. Rev. **D80**, 074020 (2009), [0907.2191](#).
- [10] M. Fabbrichesi, M. Pinamonti, and A. Tonero, Eur. Phys. J. **C74**, 3193 (2014), [1406.5393](#).
- [11] C. Bernardo, N. F. Castro, M. C. N. Fiolhais, H. Goncalves, A. G. C. Guerra, M. Oliveira, and A. Onofre, Phys. Rev. **D90**, 113007 (2014), [1408.7063](#).
- [12] Q.-H. Cao, B. Yan, J.-H. Yu, and C. Zhang (2015), [1504.03785](#).
- [13] A. Prasath V, R. M. Godbole, and S. D. Rindani, Eur. Phys. J. **C75**, 402 (2015), [1405.1264](#).
- [14] Z. Hioki and K. Ohkuma, Phys. Lett. **B752**, 128 (2016), [1511.03437](#).
- [15] C. Zhang, Phys. Rev. Lett. **116**, 162002 (2016), [1601.06163](#).
- [16] J. L. Birman, F. Dliot, M. C. N. Fiolhais, A. Onofre, and C. M. Pease, Phys. Rev. **D93**, 113021 (2016), [1605.02679](#).
- [17] E. Boos, V. Bunichev, L. Dudko, and M. Perfilov (2016), [1607.00505](#).
- [18] A. Jueid (2018), [1805.07763](#).
- [19] Q.-H. Cao and B. Yan, Phys. Rev. **D92**, 094018 (2015), [1507.06204](#).
- [20] G. A. Ladinsky and C. P. Yuan, Phys. Rev. **D49**, 4415 (1994), [hep-ph/9211272](#).
- [21] D. O. Carlson and C. P. Yuan, Phys. Lett. **B306**, 386 (1993).
- [22] D. O. Carlson and C. P. Yuan, in *Top Quark Workshop Ames, Iowa, May 25-26, 1995* (1995), pp. 172–177, [hep-ph/9509208](#).
- [23] T. M. P. Tait and C. P. Yuan, Phys. Rev. **D55**, 7300 (1997), [hep-ph/9611244](#).
- [24] C. S. Li, R. J. Oakes, and J. M. Yang, Phys. Rev. **D55**, 5780 (1997), [hep-ph/9611455](#).
- [25] C.-S. Li, R. J. Oakes, J.-M. Yang, and H.-Y. Zhou, Phys. Rev. **D57**, 2009 (1998), [hep-ph/9706412](#).
- [26] T. M. P. Tait and C. P. Yuan (1997), [hep-ph/9710372](#).
- [27] H.-J. He and C. P. Yuan, Phys. Rev. Lett. **83**, 28 (1999), [hep-ph/9810367](#).
- [28] T. M. P. Tait and C. P. Yuan, Phys. Rev. **D63**, 014018 (2000), [hep-ph/0007298](#).
- [29] E. Malkawi, T. M. P. Tait, and C. P. Yuan, Phys. Lett. **B385**, 304 (1996), [hep-ph/9603349](#).
- [30] K. Hsieh, K. Schmitz, J.-H. Yu, and C. P. Yuan, Phys. Rev. **D82**, 035011 (2010), [1003.3482](#).
- [31] Q.-H. Cao, Z. Li, J.-H. Yu, and C. P. Yuan, Phys. Rev. **D86**, 095010 (2012), [1205.3769](#).
- [32] E. Drueke, J. Nutter, R. Schwienhorst, N. Vignaroli, D. G. E. Walker, and J.-H. Yu, Phys. Rev. **D91**, 054020 (2015), [1409.7607](#).

- [33] Q.-H. Cao, X. Wan, X.-p. Wang, and S.-h. Zhu, Phys. Rev. **D87**, 055022 (2013), [1301.6608](#).
- [34] Q.-H. Cao, C. S. Li, and C. P. Yuan, Phys. Lett. **B668**, 24 (2008), [hep-ph/0612243](#).
- [35] E. L. Berger, Q.-H. Cao, C.-R. Chen, and H. Zhang, Phys. Rev. **D83**, 114026 (2011), [1103.3274](#).
- [36] E. L. Berger, Q.-H. Cao, J.-H. Yu, and C. P. Yuan, Phys. Rev. **D84**, 095026 (2011), [1108.3613](#).
- [37] S. Alekhin, S. Moch, and S. Thier, Phys. Lett. **B763**, 341 (2016), [1608.05212](#).
- [38] Tech. Rep. CMS-PAS-TOP-15-001, CERN, Geneva (2016), URL <http://cds.cern.ch/record/2138689>.
- [39] S. Alekhin, J. Blmllein, S. Moch, and R. Plaakyt, Phys. Rev. **D94**, 114038 (2016), [1508.07923](#).
- [40] G. Aad et al. (ATLAS), Phys. Rev. **D90**, 112006 (2014), [1406.7844](#).
- [41] S. Chatrchyan et al. (CMS), JHEP **12**, 035 (2012), [1209.4533](#).
- [42] M. Aaboud et al. (ATLAS), Eur. Phys. J. **C77**, 531 (2017), [1702.02859](#).
- [43] V. Khachatryan et al. (CMS), JHEP **06**, 090 (2014), [1403.7366](#).
- [44] M. Aaboud et al. (ATLAS), JHEP **04**, 086 (2017), [1609.03920](#).
- [45] A. M. Sirunyan et al. (CMS), Phys. Lett. **B772**, 752 (2017), [1610.00678](#).
- [46] M. Brucherseifer, F. Caola, and K. Melnikov, Phys. Lett. **B736**, 58 (2014), [1404.7116](#).
- [47] E. L. Berger, J. Gao, C. P. Yuan, and H. X. Zhu, Phys. Rev. **D94**, 071501 (2016), [1606.08463](#).
- [48] E. L. Berger, J. Gao, and H. X. Zhu (2017), [1708.09405](#).
- [49] S. Zhu, Phys. Lett. **B524**, 283 (2002), [Erratum: Phys. Lett.B537,351(2002)], [hep-ph/0109269](#).
- [50] B. W. Harris, E. Laenen, L. Phaf, Z. Sullivan, and S. Weinzierl, Phys. Rev. **D66**, 054024 (2002), [hep-ph/0207055](#).
- [51] Q.-H. Cao and C. P. Yuan, Phys. Rev. **D71**, 054022 (2005), [hep-ph/0408180](#).
- [52] Q.-H. Cao, R. Schwienhorst, and C. P. Yuan, Phys. Rev. **D71**, 054023 (2005), [hep-ph/0409040](#).
- [53] J. M. Campbell, R. K. Ellis, and F. Tramontano, Phys. Rev. **D70**, 094012 (2004), [hep-ph/0408158](#).
- [54] Q.-H. Cao, R. Schwienhorst, J. A. Benitez, R. Brock, and C. P. Yuan, Phys. Rev. **D72**, 094027 (2005), [hep-ph/0504230](#).
- [55] J. M. Campbell and F. Tramontano, Nucl. Phys. **B726**, 109 (2005), [hep-ph/0506289](#).
- [56] Q.-H. Cao (2008), [0801.1539](#).
- [57] S. Heim, Q.-H. Cao, R. Schwienhorst, and C. P. Yuan, Phys. Rev. **D81**, 034005 (2010), [0911.0620](#).
- [58] J. M. Campbell, R. Frederix, F. Maltoni, and F. Tramontano, Phys. Rev. Lett. **102**, 182003 (2009), [0903.0005](#).

- [59] R. Schwienhorst, C. P. Yuan, C. Mueller, and Q.-H. Cao, Phys. Rev. **D83**, 034019 (2011), [1012.5132](#).
- [60] P. Falgari, P. Mellor, and A. Signer, Phys. Rev. **D82**, 054028 (2010), [1007.0893](#).
- [61] S. Frixione, E. Laenen, P. Motylinski, and B. R. Webber, JHEP **03**, 092 (2006), [hep-ph/0512250](#).
- [62] S. Alioli, P. Nason, C. Oleari, and E. Re, JHEP **09**, 111 (2009), [Erratum: JHEP02,011(2010)], [0907.4076](#).
- [63] R. Frederix, E. Re, and P. Torrielli, JHEP **09**, 130 (2012), [1207.5391](#).
- [64] R. Frederix, S. Frixione, A. S. Papanastasiou, S. Prestel, and P. Torrielli, JHEP **06**, 027 (2016), [1603.01178](#).
- [65] S. Carrazza, R. Frederix, K. Hamilton, and G. Zanderighi (2018), [1805.09855](#).
- [66] M. de Beurs, E. Laenen, M. Vreeswijk, and E. Vryonidou, Eur. Phys. J. **C78**, 919 (2018), [1807.03576](#).
- [67] N. Kidonakis, Phys. Rev. **D74**, 114012 (2006), [hep-ph/0609287](#).
- [68] N. Kidonakis, Phys. Rev. **D75**, 071501 (2007), [hep-ph/0701080](#).
- [69] H. X. Zhu, C. S. Li, J. Wang, and J. J. Zhang, JHEP **02**, 099 (2011), [1006.0681](#).
- [70] J. Wang, C. S. Li, H. X. Zhu, and J. J. Zhang (2010), [1010.4509](#).
- [71] N. Kidonakis, Phys. Rev. **D83**, 091503 (2011), [1103.2792](#).
- [72] J. Wang, C. S. Li, and H. X. Zhu, Phys. Rev. **D87**, 034030 (2013), [1210.7698](#).
- [73] Q.-H. Cao, P. Sun, B. Yan, C. P. Yuan, and F. Yuan (2018), [1801.09656](#).
- [74] J. C. Collins, D. E. Soper, and G. F. Sterman, Nucl. Phys. **B250**, 199 (1985).
- [75] J. C. Collins and D. E. Soper, Nucl. Phys. **B193**, 381 (1981), [Erratum: Nucl. Phys.B213,545(1983)].
- [76] J. C. Collins and D. E. Soper, Nucl. Phys. **B197**, 446 (1982).
- [77] H. X. Zhu, C. S. Li, H. T. Li, D. Y. Shao, and L. L. Yang, Phys. Rev. Lett. **110**, 082001 (2013), [1208.5774](#).
- [78] H. T. Li, C. S. Li, D. Y. Shao, L. L. Yang, and H. X. Zhu, Phys. Rev. **D88**, 074004 (2013), [1307.2464](#).
- [79] R. Zhu, P. Sun, and F. Yuan, Phys. Lett. **B727**, 474 (2013), [1309.0780](#).
- [80] P. Sun, C. P. Yuan, and F. Yuan, Phys. Rev. Lett. **114**, 202001 (2015), [1409.4121](#).
- [81] P. Sun, C. P. Yuan, and F. Yuan, Phys. Rev. Lett. **113**, 232001 (2014), [1405.1105](#).
- [82] P. Sun, C. P. Yuan, and F. Yuan, Phys. Rev. **D92**, 094007 (2015), [1506.06170](#).
- [83] P. Sun, C. P. Yuan, and F. Yuan, Phys. Lett. **B762**, 47 (2016), [1605.00063](#).
- [84] P. Sun, J. Isaacson, C. P. Yuan, and F. Yuan (2016), [1602.08133](#).
- [85] B.-W. Xiao and F. Yuan (2018), [1801.05478](#).
- [86] P. Sun, C. P. Yuan, and F. Yuan (2018), [1802.02980](#).

- [87] P. Sun, B. Yan, C. P. Yuan, and F. Yuan (2018), [1810.03804](#).
- [88] P. Sun, B. Yan, and C. P. Yuan (2018), [1811.01428](#).
- [89] M. G. A. Buffing, Z.-B. Kang, K. Lee, and X. Liu (2018), [1812.07549](#).
- [90] X. Liu, F. Ringer, W. Vogelsang, and F. Yuan (2018), [1812.08077](#).
- [91] F. Landry, R. Brock, G. Ladinsky, and C. P. Yuan, Phys. Rev. **D63**, 013004 (2001), [hep-ph/9905391](#).
- [92] F. Landry, R. Brock, P. M. Nadolsky, and C. P. Yuan, Phys. Rev. **D67**, 073016 (2003), [hep-ph/0212159](#).
- [93] P. Sun, C. P. Yuan, and F. Yuan, Phys. Rev. **D88**, 054008 (2013), [1210.3432](#).
- [94] P. Sun, J. Isaacson, C. P. Yuan, and F. Yuan (2014), [1406.3073](#).
- [95] S. Dulat, T.-J. Hou, J. Gao, M. Guzzi, J. Huston, P. Nadolsky, J. Pumplin, C. Schmidt, D. Stump, and C. P. Yuan, Phys. Rev. **D93**, 033006 (2016), [1506.07443](#).
- [96] M. A. G. Aivazis, F. I. Olness, and W.-K. Tung, Phys. Rev. **D50**, 3085 (1994), [hep-ph/9312318](#).
- [97] M. A. G. Aivazis, J. C. Collins, F. I. Olness, and W.-K. Tung, Phys. Rev. **D50**, 3102 (1994), [hep-ph/9312319](#).
- [98] J. C. Collins, Phys. Rev. **D58**, 094002 (1998), [hep-ph/9806259](#).
- [99] M. Kramer, I. F. I. Olness, and D. E. Soper, Phys. Rev. **D62**, 096007 (2000), [hep-ph/0003035](#).
- [100] P. M. Nadolsky, N. Kidonakis, F. I. Olness, and C. P. Yuan, Phys. Rev. **D67**, 074015 (2003), [hep-ph/0210082](#).
- [101] A. Belyaev, P. M. Nadolsky, and C. P. Yuan, JHEP **04**, 004 (2006), [hep-ph/0509100](#).
- [102] S. Berge, P. M. Nadolsky, and F. I. Olness, Phys. Rev. **D73**, 013002 (2006), [hep-ph/0509023](#).
- [103] S. Catani, D. de Florian, and M. Grazzini, Nucl. Phys. **B596**, 299 (2001), [hep-ph/0008184](#).
- [104] A. Mukherjee and W. Vogelsang, Phys. Rev. **D86**, 094009 (2012), [1209.1785](#).
- [105] M. Dasgupta and G. P. Salam, Phys. Lett. **B512**, 323 (2001), [hep-ph/0104277](#).
- [106] M. Dasgupta and G. P. Salam, JHEP **03**, 017 (2002), [hep-ph/0203009](#).
- [107] A. Banfi and M. Dasgupta, JHEP **01**, 027 (2004), [hep-ph/0312108](#).
- [108] J. R. Forshaw, A. Kyrieleis, and M. H. Seymour, JHEP **08**, 059 (2006), [hep-ph/0604094](#).
- [109] T. Sjostrand, S. Mrenna, and P. Z. Skands, Comput. Phys. Commun. **178**, 852 (2008), [0710.3820](#).
- [110] C. Patrignani et al. (Particle Data Group), Chin. Phys. **C40**, 100001 (2016).
- [111] J. M. Campbell, R. K. Ellis, and W. T. Giele, Eur. Phys. J. **C75**, 246 (2015), [1503.06182](#).
- [112] A. Banfi, S. Redford, M. Vesterinen, P. Waller, and T. R. Wyatt, Eur. Phys. J. **C71**, 1600 (2011), [1009.1580](#).
- [113] C. Collaboration (CMS) (2016).